ACS ES&T Engineering

pubs.acs.org/estengg

Article

Modeling the Plantwide Implications of Struvite Loss from Sidestream Precipitation Reactors

Samuel E. Aguiar, Manying Zhang, Adrian Romero-Flores, Tom Johnson, and Roland D. Cusick*

Cite This: *ACS EST Engg.* 2022, 2, 874–885

Read Online

ACCESS | Metrics & More | Article Recommendations | Supporting Information

ABSTRACT: The combination of enhanced biological phosphorus removal (EBPR) with sidestream struvite precipitation is a synergistic treatment approach for P removal and recovery. However, periodic disruption events in crystallization reactors can cause fine struvite particle washout followed by P solubilization, leading to decreases in EBPR effluent quality, yet modeling tools do not exist to quantify plantwide impacts of struvite loss. To understand the impacts of struvite loss and dissolution on EBPR, this work first quantifies the dissolution rate of field-harvested struvite using the surface area-dependent shrinking object model and presents a novel particle population balance dissolution modeling tool for integration with a plantwide process simulator (SUMO). Analysis of time series P concentration data from dissolution experiments yields a rate constant of 1.14 mm min^{-1}. Simulations of intra-plant phosphorus dynamics indicate that when struvite reactors operate with a high capture efficiency, the majority of influent orthophosphate can be captured through sidestream precipitation. In the event of struvite loss, large particles would not fully dissolve and are removed through sedimentation during primary clarification without significant disruption of EBPR. In contrast, the loss of 200 μm-sized struvite particles can lead to a difference in effluent phosphate of up to 0.8 mg P/L. Our results suggest that surface area-dependent models are essential to quantify the impacts of struvite loss and that reactor design should center on particle retention, rather than conversion of soluble P to struvite.

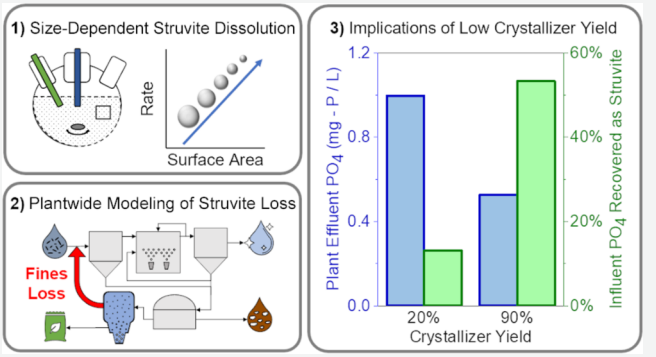

KEYWORDS: *shrinking object model, nutrient recovery, population balance modeling, fines loss, dissolution*

1. INTRODUCTION

Increasingly stringent regulatory standards for nutrients have made phosphorus management at water resource recovery facilities (WRRFs) a necessary part of treatment. By the end of 2021, 24 states and 5 U.S. territories will have implemented quantitative total phosphorus (TP) water quality standards that are used to facilitate permitting of WRRF treated effluent.[1] In Europe, even the most lenient TP limits (2 mg P/L) require specialized P treatment to achieve satisfactory effluent quality.[2,3] To reduce the P loading contribution from WRRFs,[4,5] mitigate the impact of intraplant P cycling,[6,7] and meet regulatory requirements,[1−3,8] new treatment techniques have focused on not just removal but also recovery of P from wastewater.

Enhanced biological phosphorus removal (EBPR) coupled with solids digestion and P crystallization has emerged as a sustainable approach for P removal and recovery.[9−11] P crystallization technologies operate synergistically in the sidestream, recovering P as struvite and reducing intraplant cycling of P, which can enable mainstream EBPR to attain low effluent P (~0.3−1 mg/L) without reliance on exogenous carbon.[12] However, an often overlooked practical limitation of crystallization is the nucleation and washout of fine crystals[13] that when recycled to the WRRF headworks can disrupt mainstream EBPR operations as they dissolve. This is mirrored in the academic literature, where a majority of struvite work focuses on soluble P removal through crystallization with limited data available on how much P is actually harvested from a reactor as a fraction of influent TP. From laboratory studies, the potential for fines loss on larger scales is evidenced mainly in particle size distributions (PSDs) that often are populated with crystals smaller than 200 μm.[14−25] Although crystallization reactors can be designed to account for some amount of fines production through seeding[13,21,22,26,27] or operational controls and conditions,[15,18,19,28] pilot and full-scale studies indicate the prevelance of fines washout. In pilot struvite crystallization systems, reported P removal is good

Received: November 3, 2021
Revised: March 4, 2022
Accepted: March 7, 2022
Published: March 16, 2022

https://doi.org/10.1021/acsestengg.1c00404
ACS EST Engg. 2022, 2, 874–885

ranging from 78 to 93% while recovery varies from 7 to 91% mainly due to fines loss.[29−31] Full-scale struvite crystallization systems also report fines issues with one plant producing up to 70% of its total struvite as fines (self-defined as particles <0.5 mm) depending on the operating conditions[32] and others estimating a P recovery of only 22%.[33] The continued body of evidence for fines points toward a phenomenon that is inherent to the interdependence of reactor design, operating conditions, and struvite growth mechanisms.

Assuming that most crystallizer systems will have some degree of fine particle washout, the plantwide sensitivity to P recycling would dictate whether steps should be taken to further capture these solids or implement mitigation strategies to protect effluent quality. A recent sensitivity analysis of an EBPR plantwide model showed that the dissolution rate of lost struvite is a dominant factor in determining plant effluent P, especially in cases of low solids retention in the crystallization reactor.[34] However, the general precipitation framework[35] used in the study only considers solution supersaturation and total mass rather than the surface area of solids. For sparingly soluble salts like struvite, whose crystal growth and dissolution kinetics are limited by the surface area, a model which takes the total solute area into account would elucidate the importance of particle size on dissolution rate and enable the design and operation of struvite precipitation reactors that minimize the risk of washout.[36,37]

A lack of agreement exists in the literature on the base assumptions necessary to correctly model dissolution and precipitation processes at WRRFs. Since the introduction of a strictly thermodynamics-based model for precipitation,[38] many studies have built upon mass-based frameworks for use in plantwide modeling.[35,37,39,40] Although the models included in these studies have been shown to fit equilibrium results well, they lack the ability to predict crystallizer effluent PSDs. The inclusion of a population balance equation, known as population balance modeling (PBM), allows for prediction of crystallizer effluent PSDs and can include nucleation, crystal growth, and aggregation.[17,22−25,28,41,42] Unlike the mass-based activated sludge models (ASMs),[43] the PBM tracks particle size and number to estimate area dependent growth and dissolution. Improvements have been made to struvite PBM by choosing mass as the internal coordinate and including the effects of shear on nucleation and growth.[23,25,28] Despite these improvements, difficulties still exist in accurately calibrating the PBM and even within a set of specifically chosen case studies, collinearity between kinetic parameters causes identifiability issues (i.e., model outputs must be model input-sensitive and the influence of a change in one input parameter on the model output cannot be reversed through a change in another input parameter). Unless steps are taken to isolate mechanisms, an uncommon feature in most studies in this area, it is possible that struvite precipitation data reported may be based on conditions that would be considered unidentifiable from a PBM perspective. Irrespective of the complexity in tracking particles or mass of struvite, all available models assume that precipitation and dissolution occur through the same mechanisms. This yields no difference in dissolution/precipitation rate constants at equal super-/under-saturations, often disregarding the effect of particle size and surface areas, resulting in a crucial data gap related to struvite dissolution kinetics. Second, struvite-related PBM research has been solely focused on providing a comprehensive crystallizer process modeling without quantification of implications for downstream processes during washout or upset events.

In this study, we propose the use of the shrinking object model (SOM)[44] to capture the link between phosphate mineral dissolution and solids surface area. We then integrate the SOM into a larger plantwide model to determine the effects of fine particle washout on mainstream processes. The SOM was derived using classical chemical kinetic assumptions that focus on observation rather than assumed mechanisms. In this study, the SOM is used rather than a thermodynamics-based approach to determine the dissolution rate of field-grown struvite to allow for deviation from pure struvite dissolution kinetics. Understanding struvite dissolution kinetics will allow kinetics-based plantwide models to predict the impact of fines loss on overall plant performance. The objectives of this study are to (1) fully characterize the dissolution rate of field-recovered struvite using the solute surface area-dependent SOM and (2) determine the plantwide implications of low-yield struvite precipitation and fines washout by integrating a dissolution-focused PBM into a plantwide process modeling software package.

2. MATERIALS AND METHODS

Laboratory-scale batch experiments were performed to determine the dissolution rate of field-harvested struvite samples of various particle diameters. Time series phosphorus concentration data were fit using the SOM to determine an empirically derived dissolution rate constant for struvite. Then, a PBM process model was created that included discrete struvite particle size classes with SOM-based dissolution rate equations and integrated with SUMO,[45] a plantwide process modeling software that accounts for typical biological and physio-chemical reactions present in activated sludge systems. This process model was used to determine the plantwide implications of low-yield struvite precipitation and fines washout.

2.1. Kinetic Dissolution Modeling. Following the strict empirical kinetics basis argued by Truesdale and Greenwood,[44] the SOM is used to model the dissolution of struvite.

$$\frac{dC}{dt} = k\frac{A}{V}(C_{sat} - C) \quad (1)$$

Here, C and C_{sat} are the concentrations of dissolved PO_4−P in solution and at equilibrium, respectively, A is the surface area of the solute, V is the volume of the solvent, and k is the dissolution rate constant. By integrating eq 1 under the assumption of constant A, V, and C_{sat}, a linearized expression is created (eq 2) that can be used to determine the dissolution rate constant from empirical concentration time series data.

$$-\ln(C_{sat} - C) = k\frac{A}{V}t \quad (2)$$

To satisfy the requirement of constant A, V, and C_{sat}, high struvite mass loadings, small sample collection volumes, and pH buffer were used as described in Section 2.3.

2.2. Field-Grown Struvite Samples and Preparation. Multiple sources of field-grown struvite granules were tested in this study. Following the convention of struvite granules produced in Ostara Pearl (Ostara Nutrient Recovery Technologies Inc., Vancouver, BC, Canada) reactors, particles of a diameter, D, are presented in this work according to their sieve size guide number (SGN)

https://doi.org/10.1021/acsestengg.1c00404
ACS EST Engg. 2022, 2, 874−885

$$\text{SGN } X = D \text{ (mm)}*100 \quad (3)$$

When necessary, an identifier A/B will be added when referencing a single run from a set of duplicate experiments. The first set of samples tested was from the Clean Water Services (CWS) Durham facility in Tigard, Oregon. These samples were generated in an Ostara Pearl reactor with struvite particle diameters ranging from 4.5 mm (SGN 450) down to mixed-sized dust that passed a 350 μm sieve (dust). The second set of samples was from an Ostara Pearl reactor at the Stickney Water Reclamation Plant (Stickney) in the Metropolitan Water Reclamation District of Greater Chicago. These struvite particle diameters ranged from 3.0 mm (SGN 300) down to mixed-size dust that passed a 350 μm sieve (dust). The final set of samples was from a MagPrex (formerly known as "AirPrex") pilot reactor (Centrisys/CNP, Kenosha, WI) at the Metro Wastewater Reclamation District (MWRD) in Denver, Colorado, which generated particles with a 125 μm diameter. All struvite solids were degassed in a vacuum oven (Thermo Scientific Lindberg/Blue M) at 40 °C and ambient pressure in loosely packed inert plastic containers for 2 weeks (daily manual mixing) to remove volatile organics without decomposing struvite.[46] Reference struvite solids are described in Section S1. Material characterization by X-ray diffraction (XRD) and Fourier transform infrared spectroscopy (FTIR) for all samples tested is further described in Section S2.

2.3. Dissolution Experiments. Short-term dissolution tests were conducted to determine the dissolution rate constant of the various-sized solids tested. By fitting the increasing concentration of PO_4^{3-} to the SOM, the dissolution rate constant was elucidated. The solids described in Section 2.1 were tested in duplicate short-term batch dissolution experiments. A 500 mL three-neck flask (Figure 1) was first triple-rinsed in DI water, followed by a HCl acid rinse, and finally a Tris buffer rinse. Then, the flask was filled with 450 mL of 500 mM Tris buffer (prepared as described in Section S3). A sampling needle and a calcium-ion selective electrode (Sension+ 9660 Calcium ISE) were inserted into separate outer flask necks and sealed with air-tight silicone stoppers. The solution was then sparged with N_2 and mixed with a magnetic stir bar for 10 min to remove any dissolved CO_2. The pH of the solution was checked at the beginning and end of experiments to ensure that a pH of 7.5 ± 0.02 was maintained. An initial 2 mL sample was collected before solids addition to account for any residual P in the vessel from previous experiments. Residual P was minimal in all cases and did not affect the results of these experiments.

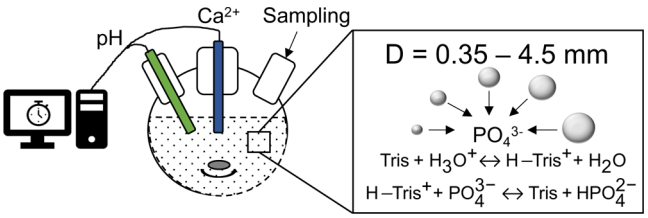

Figure 1. Short-term dissolution apparatus. The pH probe is only inserted at the beginning and at the end of short-term dissolution experiments and is sealed otherwise.

Each experiment began with the addition of struvite particles to the reaction vessel. Solids were added to the dissolution vessel at a 10 g/L loading to ensure that the total particle surface area was nearly constant over the course of the experiment, satisfying the constant surface area condition of eq 2. The vessel was then completely closed to the atmosphere and mixed with a magnetic stir bar at a rate of 300 rpm. A 2 mL sample was collected at 10 min intervals over the experiment duration of 60 min. Over the course of the experiment, only 16 mL (ΔV < 4%) was removed, thus minimizing the error associated with the constant volume assumption of eq 2. Collected liquid samples were passed through a 0.22 μm filter and analyzed for inorganic phosphate using ion chromatography (IC) (Dionex ICS-2100) with a Dionex IonPac AS18 column (Section S4). Near-real-time (5 s intervals) free calcium (Ca^{2+}) concentrations monitored with a calcium ISE showed no appreciable calcium dissolution.

Visual MINTEQ 3.1[47] was used to simulate the solution chemistry at equilibrium in the dissolution reactor to estimate a theoretical C_{sat}. It was assumed that the equilibrium behavior of the field-recovered granules would mirror that of pure struvite. However, due to the fine size and hygroscopic nature of the reference struvite, a time series dissolution curve could not be accurately collected. Instead, solids were added to a small test tube with the same buffer solution used in the short-term dissolution experiments and were left to come to equilibrium for 1 month. Periodic manual mixing ensured diffusion did not limit dissolution. Before the sample was collected for analysis, a final mixing was carried out and it was allowed to settle for 1 h. In this test, the solution reached an

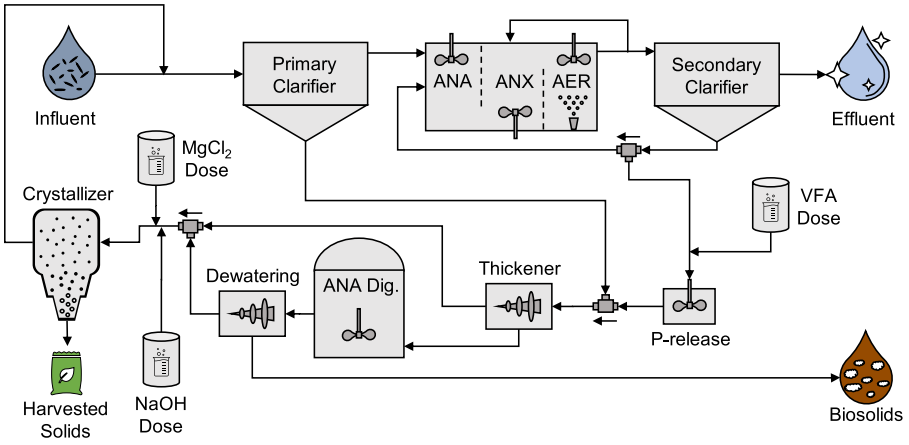

Figure 2. Process flow diagram for plantwide model simulations of struvite recovery and dissolution in SUMO.

https://doi.org/10.1021/acsestengg.1c00404
ACS EST Engg. 2022, 2, 874−885

Table 1. Stoichiometry of Discrete Particle Dissolution Processes[a]

process	S_{NH_x}	S_{PO_4}	S_{Mg}	$X_{STR,i-1}$	$X_{STR,i}$
$X_{STR,i}$ to $X_{STR,i-1}$	$\frac{(V_{STR,i}-V_{STR,i-1})}{V_{STR,i}} * \frac{AM_N}{MM_{STR}}$	$\frac{(V_{STR,i}-V_{STR,i-1})}{V_{STR,i}} * \frac{AM_P}{MM_{STR}}$	$\frac{(V_{STR,i}-V_{STR,i-1})}{V_{STR,i}} * \frac{AM_{Mg}}{MM_{STR}}$	$\frac{V_{STR,i-1}}{V_{STR,i}}$	−1
$X_{STR,i}$ to solubles	$\frac{AM_N}{MM_{STR}}$	$\frac{AM_P}{MM_{STR}}$	$\frac{AM_{Mg}}{MM_{STR}}$		−1

[a]Where S_{NH_x}, S_{PO_4}, and S_{Mg} are soluble concentrations of NH_4−N, PO_4−P, and magnesium; $V_{STR,i}$ is the volume of the ith particle; AM_N, AM_P, and AM_{Mg} are the atomic mass of N, P, and Mg; and MM_{STR} is the molecular mass of struvite. It is important to note that this framework does not change how precipitation or growth proceeds. Although this is an important component for modeling the crystallization process, we opted to use the built-in precipitation rate equations (based on saturation alone) and assumed that only particles of a defined single size exited the crystallizer reactor in all cases to focus on the impacts of particle size, yield, and dissolution because these are the parameters that will impact EBPR efficacy.

empirical $C_{sat,exp}$ of 6.14 mM P measured by IC. $C_{sat,exp}$ was used later when fitting time series results to the SOM. This simulation was also used to determine if the solution conditions of the proposed dissolution experiments would result in the saturation of other P-containing solids. In addition to the solids considered in Visual Minteq V3.1, Cattite (pK_{sp} = 23.1)[48] was added as a potential forming solid. Ruling out the formation of other solids is necessary to ensure that the dissolution rate constant found is directly linked to dissolution of struvite and not the net rate of P appearance during simultaneous precipitation of another solid. Section S5 (Figure S3) shows that over the course of the experiment, no other P-containing solids were supersaturated during the dissolution experiments.

2.4. Plantwide Modeling and Simulation. All process modeling and simulation studies were performed using SUMO v19.3 by Dynamita. To integrate the effect of particle size on struvite dissolution, 100 new state variables that represented discrete struvite particle sizes were added to the default SUMO1 kinetic model—an activated sludge model that includes one-step denitrification, polyphosphate accumulating organisms (PAO), glycogen accumulating organisms, and mineral precipitation. Each of the particles follows the generic particle functions/reactions described in Section 2.4.1.

The particles added ranged in diameter from 1 to 1000 μm to represent fines up to harvest-ready solids. A generic plant layout based on a A2O mainstream treatment chain for N and P removal with sidestream solids handling and struvite precipitation shown in Figure 2 was used.

2.4.1. Generalized Discrete Particle Functions. To account for size-specific struvite dissolution rates, additional reactions were added to the Gujer kinetic matrix (SUMO1) based on the SOM. These reactions can be generalized into either (A) solids to solids + ions or (B) solids to ions. In our system, only the smallest size class follows reaction (B), while all other particles follow reaction (A). The rate at which particles dissolved and changed from size class i to $i-1$ was calculated according to a discretized SOM (eq 1). Because mass is used to track state variables in SUMO, eq 4 is used to calculate surface area concentration per particle.

$$\left(\frac{A}{V}\right)_i = X_{STR,D_i}\left(\frac{1}{\rho}\frac{SA_i}{V_i}\right) \quad (4)$$

where X_{STR,D_i} is struvite mass concentration and SA_i is the surface area of the ith particle. The volume of solution is V_i. The density of the particles is ρ. Finally, $(A/V)_i$ is the surface area concentration per particle. The stoichiometry of the two generalized reactions is given in Table 1.

2.4.2. Influent Wastewater Composition. In all cases, the influent conditions were selected according to default parameters set in SUMO. An abbreviated influent characterization is shown in Table 2. A further breakdown of the influent composition into the state variables accepted by the modified SUMO1 model used is given in Table S1.

Table 2. Base Case Influent Characterization

parameter	influent concentration	unit
flow rate	24 000.0	m^3/d
temperature	20.0	°C
total COD	420.0	g COD/m^3
total BOD_5	183.2	g O_2/m^3
TSS	183.0	g TSS/m^3
VSS	155.3	g VSS/m^3
TN	34.4	g N/m^3
NH_4−N	24.0	g N/m^3
NO_x−N	0.0	g N/m^3
TP	4.3	g P/m^3
PO_4−P	2.5	g P/m^3
Mg	15.0	g Mg/m^3
Ca	15.0	g Ca/m^3

2.4.3. Plantwide Design and Operating Parameters. HRT and SRT for primary clarification, A2O EBPR, and anaerobic digestion were set to generally accepted values given in Metcalf and Eddy.[49] Default operating parameters in SUMO v19.3 were used, where recommendations in Metcalf and Eddy were not given. Table S2 lists HRT, SRT, and necessary operating parameters for all units shown in Figure 2.

2.4.4. Primary Clarification—Reactive Volume and Point Separator. To allow for dissolution to occur in the primary clarifier, a dual-stage process was created, where stage 1 acts as a biologically inactive CSTR that allows for struvite dissolution and stage 2 is a volumeless point separator clarifier. In this arrangement, it is assumed that real-world dissolution processes are independent of settling or any accumulation of struvite in an existing sludge blanket that may alter the overall dissolution rate. This method also assumes that any solubilized P is distributed proportionally to the flow of liquid effluents and primary sludge. Although previous frameworks[50] show that particles in the size range simulated (1−1000 μm) should have size-dependent settling rates, we do not have sufficient data to quantify this difference in struvite. Considering this lack of data, we have assumed a constant percentage removal of TSS across all simulated size classes.

2.4.5. P Release, Anaerobic Digestion, and Sludge Thickening. Following primary clarification and biological

https://doi.org/10.1021/acsestengg.1c00404
ACS EST Engg. 2022, 2, 874−885

treatment, the produced sludge is sent to a solids treatment train. Sludge from the secondary clarifier containing EBPR biomass is first passed through an anaerobic CSTR (based on Ostara WASSTRIP)[51] with an HRT of 1 h to solubilize polyphosphate fixed in PAO biomass. Next, this P-stripped secondary sludge and primary sludge are combined and thickened, sent to an anaerobic digester, and finally dewatered. The nutrient-rich liquid fractions resulting from thickening and dewatering are combined and sent to the struvite crystallizer (Figure 2). We assume 100% solids removal during thickening and dewatering to simplify the struvite particle mass balance and reduce complexity of the system. This assumption allows for easier tracking of struvite particles within the plant and does not pose cases where fully recycled particles may begin to grow again in the crystallizer. Although this may artificially increase biosolids struvite, the effect is minimized due to a small increase in percentage removal compared to the default value. The anaerobic digester is set to 35 °C.

2.4.6. Crystallizer Conversion and Yield Conditions. In all simulations, conversion of PO_4−P to struvite in the crystallizer was set at ∼90% of influent PO_4−P mass[52,53] by increasing the local precipitation rate constant sufficiently high such that conversion was controlled by equilibrium rather than kinetics. Although this is near the upper range of P removal reported in the literature, this allows for easier understanding of the importance of yield—a much harder to control process variable than conversion. The pH of the crystallizer was set to 8.5 by dosing NaOH, and the Mg/P molar ratio was set to 1:1 by dosing $MgCl_2$. Yield in the crystallizer is defined as

$$\text{yield} = \frac{M_{\text{STR,Cryst}} - M_{\text{STR,Cryst,Eff}}}{M_{\text{STR,Cryst}}} * 100 \quad (5)$$

where $M_{\text{STR,Cryst}}$ is the total mass of struvite precipitated in the crystallizer and $M_{\text{STR,Cryst,Eff}}$ is the mass flow of struvite in the crystallizer effluent. In all simulations, yield was set manually by removing all struvite solids in the crystallizer effluent and redosing with struvite particles of the desired size. Due to the difficulties in selecting an applicable PBM calibration for struvite precipitation as described earlier,[23] we instead chose to rely on an assumed crystallizer effluent PSD. Similarly, a high solids retention efficiency of the thickeners stops the recirculation of struvite acting as seed material for new growth, negating the need for a size-dependent growth model although recent PBM work has shown that this can be carried out.[23,25,28]

3. RESULTS AND DISCUSSION

3.1. Quantifying the Dissolution Rate of Field-Grown Struvite. Observed dissolution of struvite harvested from field reactors generally exhibited an inverse relationship to granule size (Figure 3A). The time series P concentration data collected during dissolution experiments were fit according to the linearized SOM (Figure 3B). A mean dissolution rate constant of 1.14 mm min^{-1} was calculated from experimental data. A best fit line is also given for the slowest and fastest dissolving particles at 0.94 mm min^{-1} (Stickney 90) and 2.61 mm min^{-1} (CWS 300), respectively. This deviation is small relative to the multi-order of magnitude differences reported for past precipitation studies, typically in which particle size was not considered.[13] Figure 3 only shows data for solids (CWS 90, 150, 300, and 450; Stickney 90, 150, and 300), whose C_{sat} approached that of the reference pure struvite (6.14 mM P). XRD (Figure S1) and FTIR (Figure S2) spectra for

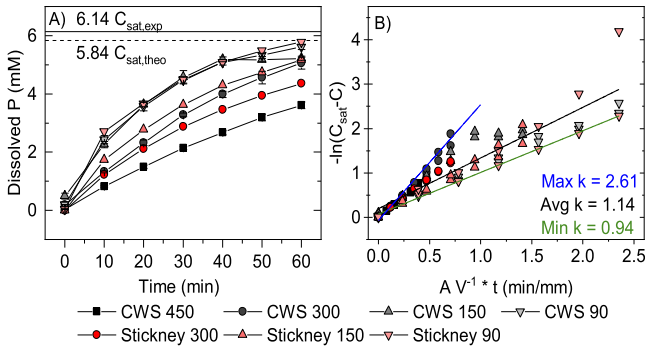

Figure 3. (A) Phosphate concentration data from dissolution experiments. All data reported are from samples which did not exceed the theoretical solubility of struvite and had well-defined size. (B) Dissolution data was fit to the SOM. An average dissolution rate of 1.14 mm min^{-1} was found with lower and upper bounds of 0.94 mm min^{-1} (Stickney 90) and 2.61 mm min^{-1} (CWS 300), respectively.

these solids were all similar to those of the reference pure struvite. Samples that exceeded the expected solubility of pure struvite were shown to contain other impurities either believed to be extraneous P-containing solids or organic surface impurities and were not included in the kinetic modeling of plantwide struvite dissolution (Figure 3). The complexities of struvite−organic interactions are intentionally avoided through low-temperature degassing to volatilize any surface organics on the solids (Section 2.2). However, struvite crystallization and dissolution will occur in the presence of organic matter and cannot be ignored. Furthermore, discussion on these interactions is given in Section 3.4, where samples that showed excess solubility relative to pure struvite are attributed to either organic or inorganic impurities using FTIR and XRD. Using the SOM, plantwide process modeling can now account for surface area-dependent dissolution of struvite. In the following sections, we discuss the plantwide implications for struvite precipitation and dissolution processes as a function of yield and particle size.

3.2. Struvite Dissolution in Primary Clarification. Steady-state simulations at constant crystallizer yield typical of working field reactors (43.5%) were run across various particles sizes to determine overall dissolution rates when mixed with the plant influent prior to primary clarification. Simulation data showed a clear size-dependent relationship between the dissolution rate and the amount of struvite available for settling in the primary clarifier (HRT of 2 h), confirming the importance of PBE equations in modeling struvite at WRRFs (Figure 4). For 1000 μm particles, nearly 80% of the influent solids survive dissolution in the reactive volume (stage 1) of the clarifier. This decreases to less than 10% for struvite particles smaller than ∼200 μm in diameter. The following sedimentation stage then clearly poses a second difference in the removal mechanism between large and small particles. For large particles, Figure S5 shows that of the 1000 μm particles that do not dissolve in the primary clarifier (16.3 kg P/d), 60% (9.8 kg P/d) are removed through sedimentation while the rest continue to mainstream EBPR for further dissolution in the A2O process. In contrast, Figure S6 shows that for 200 μm struvite, particles are almost entirely solubilized, with only 1.5 kg P/d being removed through sedimentation. Understanding if the removal mechanisms simulated in the primary-clarification two-stage system

https://doi.org/10.1021/acsestengg.1c00404
ACS EST Engg. 2022, 2, 874−885

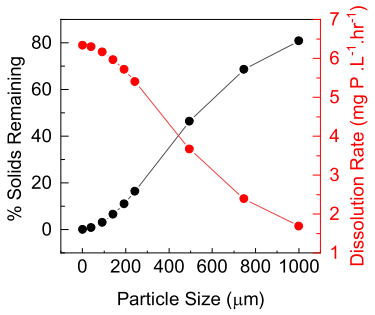

Figure 4. % Solids remaining and P dissolution rate in the liquid phase after dissolution in the primary clarification (HRT = 2 h) before sedimentation.

continue in the reactive A2O treatment chain followed by secondary clarification provides insight into the fate of P flows that continue from primary treatment.

Although the effluent mass flows are larger for small particles as compared to large particles, one commonality is the lack of struvite solids at typical operating yields in both plant effluents (Table S3) and secondary sludge (Figures S5 and S6). This means that for the conditions simulated, sufficient HRT and driving force for P uptake are available in the A2O process to sequester most PO_4−P and dissolve any surviving solids from the primary clarifier. However, the efficacy of P uptake in the mainstream relies on the assumption that a sufficient BOD/P ratio exists in the influent, allowing EBPR to metabolize influent P and remove P through biomass sedimentation. The sensitivity of this assumption is displayed when comparing the effluent P mass flows shown in Table S3 between 1000 and 200 μm particles at 43.5% yield. For the smaller particles which tend to dissolve and release PO_4−P in primary clarification, a 15% and 22% increase in TP and PO_4−P effluent mass flow originates from this reduction in BOD/P. Nearly 22% more PO_4−P is present in the mainstream EBPR feedstock compared to the large-particle scenario but lacks additional carbon dosing to compensate.

It should be noted that the point separator clarification model used in this analysis gives no preference to sedimentation of larger particles although higher settling rates would likely exist in real operation.[50] Smaller particles that may tend to remain in solution dissolve at extents larger than observed in simulation here. Other studies have shown fines[19] to be smaller than the 200 μm particles simulated, indicating complete dissolution of lost struvite is plausible during primary clarification. P in excess of what is present in the influent can reduce EBPR efficacy if the BOD/P ratio is sufficiently altered.[49] Additional data is shown in Section S6 for this system, where the BOD/P ratio is decreased to demonstrate P breakthrough and its effects on effluent quality. The likelihood of P breakthrough is limited under simulated conditions but is dependent on the influent BOD/P ratio and additional P mass flow returning from the crystallizer and dissolving in the primary clarifier.

3.3. Impact of Yield and Particle Size on Effluent Quality and Fate of P. To elucidate the effect of struvite crystallizer yield on treated effluent quality and the fate of P in all plant effluent flows (treated effluent, biosolids, and harvested struvite), two sets of steady-state simulations were run across various yields with an assumed unimodal particle size in the crystallizer effluent of 200 and 1000 μm (Figure 5).

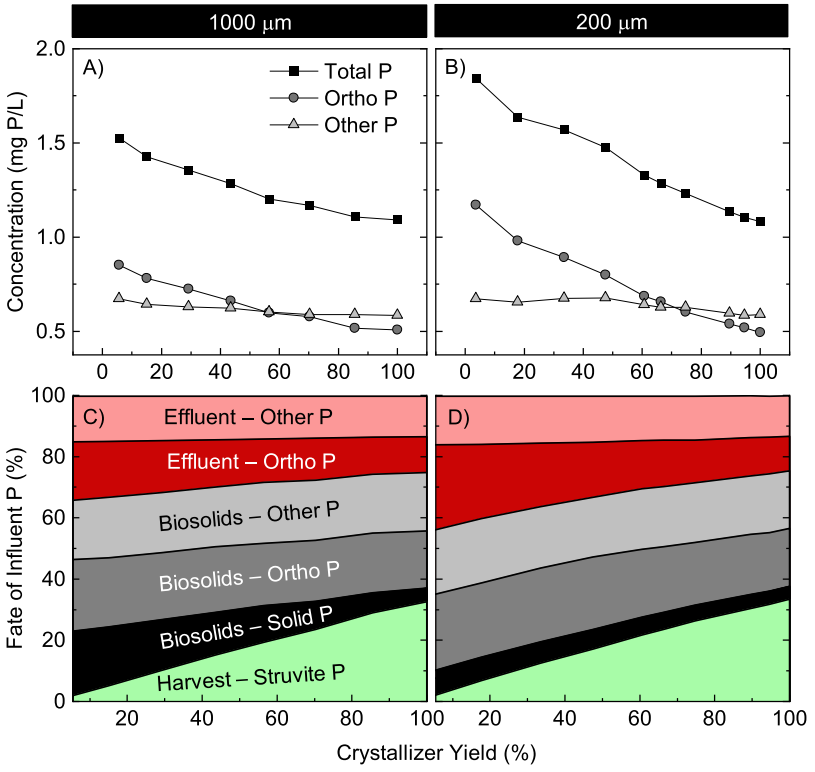

Figure 5. Effluent quality (A,B) and fate of P (C,D) for 1000 (A,C) and 200 μm (B,D) particles, respectively. In both (A,B), effluent struvite concentrations were very low (~10^{-4} g/L) and are therefore not shown. Amorphous calcium phosphate (ACP) accounts for approximately 4% of the P mass labeled "biosolids—solid P" with struvite forming the remainder in both (C,D).

https://doi.org/10.1021/acsestengg.1c00404
ACS EST Engg. 2022, 2, 874−885

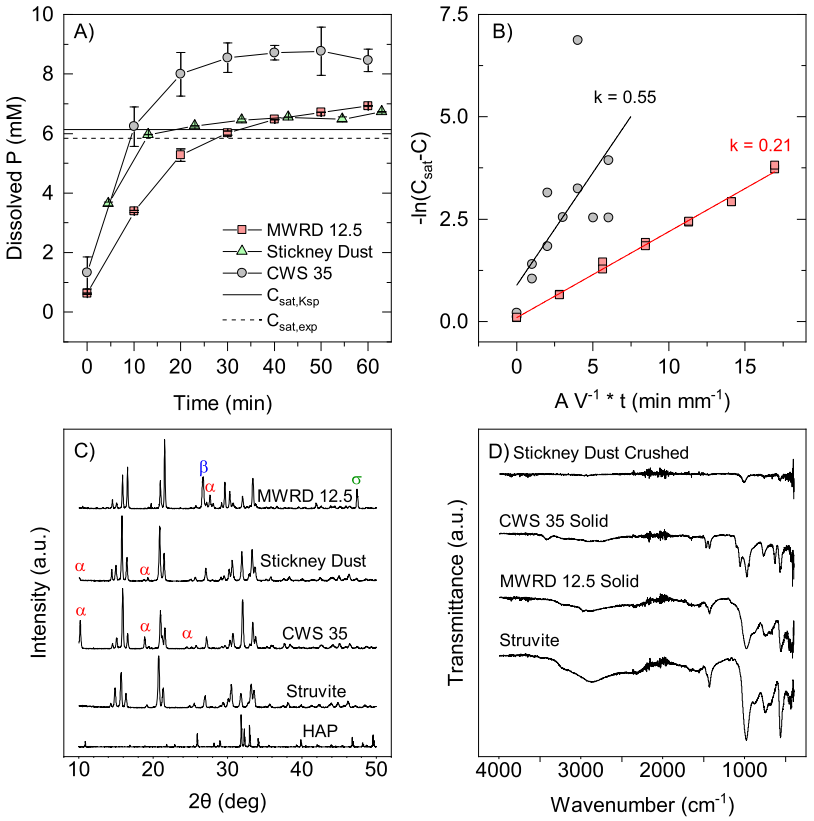

Figure 6. (A) Phosphate concentration data from dissolution experiments for particles that exhibited higher solubility than experimentally determined struvite solubility. $C_{sat,theo}$ = 6.14 mM P and $C_{sat,exp}$ = 5.84 mM P. (B) Raw data fit to the SOM. Stickney dust is excluded because particle size was not well-defined. (C) XRD of solids which featured distinct crystalline phases other than struvite. Characteristic peaks are marked as follows: dittmarite—α, quartz—β, and unidentified—σ. (D) FTIR spectra from a reference struvite sample and excess solubility solids.

The 1000 μm particle was representative of the dissolution data collected in this study while the 200 μm particle represented a particle size in which 90% of lost solids would dissolve during primary clarification and represent the upper limit of the particle size class that is expected to be lost from working struvite precipitation reactors.[19]

Regardless of particle size, the main driver of changes in effluent TP across yields is PO_4–P (ortho P) (69 and 89%, respectively, Figure 5A,B) from the dissolution of struvite when carbon is not limiting EBPR P uptake. For the 200 μm particle condition, a difference of up to 0.8 mg/L P is observed in the treated wastewater effluent between full washout and 100% yield (Figure 5A), representing a 62% increase in daily effluent P mass flow (Table S3). Even for the 1000 μm particle conditions, the difference in effluent TP between the full washout and 100% yield cases is 0.45 mg/L P (Figure 5B). For plants that have implemented P removal processes like EBPR and P crystallizers to meet stringent permit limits, these changes in effluent concentration show the clear benefit of sidestream struvite recovery but also highlight how precipitation-upset events could cause EBPR disruption and permit exceedances.

Next, the concentration and form of P at each outlet from the previously described simulation was analyzed to determine the fate of influent P as a function of yield (Figure 5C,D). The three plant outlets are referred to as "effluent", "biosolids", and "harvest", which describe the plants product water, biosolids wasting, and the struvite crystallizer harvest line, respectively. All P is categorized as ortho P, solid P (struvite + ACP), and other P (which can be thought of as any other potential P sinks but is almost exclusively sludge biomass). When crystallizer yield was high, regardless of fine particle size, the majority of influent P was recovered as harvested struvite (Figure 5C,D), highlighting the synergistic effect of EBPR and sidestream struvite precipitation for P removal and recovery. However, operating at yields typical of high-performance crystallizers (40–60%) results in similar P mass flows in both harvested struvite and biosolids ortho P.

To capture the majority of PO_4–P as harvested struvite, yield must exceed the current standards of operation. For both 1000 and 200 μm simulation cases, the majority of TP exits the plant in the biosolids across all yields. As yield decreases, more P as struvite is recycled to the headworks, leading to dissolution as loss in the plant effluent or capture in biosolids. Since the dissolution kinetics is greater for 200 μm crystals, more dissolution occurs in the primary clarifier, which lowers the solid P fraction in biosolids while reducing EBPR efficacy due to reduced BOD/P (Figure 5C,D). However, this result depends partially on the assumption of 100% solids retention in the thickener and dewatering systems. This value surpasses typical operation but was used to stop recirculation of struvite back to the crystallizer after washout. Including recirculation would warrant the inclusion of a PBM-based struvite crystallization model that is outside of the scope of this work but does limit the accuracy of the fate results shown. These results highlight how designing struvite crystallization reactors to maximize yield would have impacts on EBPR performance, biosolids composition, and struvite accumulation in anaerobic digesters.

https://doi.org/10.1021/acsestengg.1c00404
ACS EST Engg. 2022, 2, 874–885

3.4. Physical and Chemical Differences of Field-Grown Struvite and Excess Solubility. Impurities can alter the dissolution behavior of struvite particles either by reducing the true struvite surface area, releasing P in excess of what would be expected for dissolution of pure struvite, or adsorbing to the surface creating diffusion barriers. In this study, three of the field-collected solids, namely, MWRD 12.5, Stickney dust, and CWS 35, exhibited excess solubility compared to reference struvite (Figure 6A). Impurities in recovered solids from struvite crystallization are not uncommon as K analogues exist[54−56] and naturally present Ca forms insoluble phosphate solids that compete with Mg.[52,53,57,58] Additionally, the presence of soluble and particulate organic matter in crystallizer feedstock streams could also interact with particle surfaces, although their interaction with struvite is poorly understood.[59−61] When comparing the dissolution rate constants shown in Figures 3B−6B, we see much smaller dissolution rate constants that indicate an intrinsic difference between the solids, likely related to composition. Stickney dust is excluded from Figure 6B because the sample did not have unimodal PSD. Without this information, estimates for the total surface area and fitting to the SOM are not possible.

Experimental evidence indicates that differences in the crystal phase or interactions with other organic impurities can lead to differences in equilibrium solubility and dissolution kinetics. XRD and FTIR were used to determine if inorganic or organic impurities were present and potentially contributed to observed differences in particle dissolution. In XRD spectra collected for CWS SGN 35, three extraneous peaks were detected at 10.2, 18.8, and 24.5° and identified as dittmarite ($MgNH_4PO_4{*}H_2O$, Figure 6C). In Stickney dust, dittmarite peaks were found at 10.2 and 18.8°. Dittmarite in Stickney dust can partially be attributed to dehydration during harvesting or sample prepration. However, this heating step is not present in CWS SGN 35 or larger particles, implying that dittmarite may form under typical struvite crystallizer conditions. MWRD 12.5 was more complex with a dittmarite peak at 27.6°, a quartz peak at 26.7°, and an unidentified but strong peak at 47.38°. The quartz impurities in MWRD 12.5 are expected due to residual sand present from the struvite harvesting method of that specific reactor. All other samples tested were nearly identical to the struvite reference solid with some slight peak shifting attributed to strain within the crystals.[62,63] No significant peak matches were made with reference hydroxyapatite in any of the field-grown samples.

Differences were also observed in the FTIR spectra of solids that exhibited excess solubility (Figure 6D). In this analysis, the objective is not to find specific compounds, which may be present in the samples through fingerprint analysis, but to show common group frequencies shared within the samples and contrast them with those of the reference struvite sample. This serves to develop an understanding of what types of molecules may alter the dissolution behavior from pure struvite either through molecules adsorbed on the surface of the field-recovered struvite or in solution acting as a dissolution inhibitor. Crushed samples give general chemistry of the solid, and "solid" samples give surface character.

As a reference sample, the pure struvite is expected to contain only inorganic PO_4^{3-} (very strong at 1030 cm^{-1} and medium at 570 cm^{-1}) and NH_4^+ (strong at 1410 cm^{-1}) FTIR bands.[64,65] In fact, the reference struvite does contain inorganic IR bands at 1430 and 560 cm^{-1} (Figure 6D). However, medium-strength broad peaks also appear at 2330, 2870, 3220 cm^{-1}, and very weakly at 3500 cm^{-1}, strengthening the indication of a primary amine (doublet at 3380 and 3300 cm^{-1} and a strong peak at 3000−2700 cm^{-1}) or of a secondary amine (a broad strong peak at 2700−3000 cm^{-1} and a medium-strength peak at 1620−1560 cm^{-1}).[64] The MWRD 12.5 sample matches the reference struvite spectra in both crushed and solid samples (Figure S2). The surface sample of CWS SGN 35 was very distinct from the reference struvite spectra with a weak peak at 3420 cm^{-1}, a doublet at 2900 and 2750 cm^{-1}, and a distinct fingerprint region. This could again describe a primary amine by fulfilling 3500−3300, 3400−3200, 1630−1590, and 900−600 cm^{-1}.[64] Crushed CWS SGN 35 spectra were nearly identical to the reference struvite spectra (Figure S2). In contrast, solid Stickney dust (Figure S2) matches the reference struvite while the crushed sample only exhibits a weak peak at 1000 and 570 cm^{-1}. Definitive conclusions are hard to draw from this sample in terms of what species the fingerprint region indicates, but an absence of upper bands present in the reference struvite is clear.

In all cases, the differences in the FTIR spectra relative to the reference struvite indicate potential organic impurities both on the surface and integrated into the recovered solids. Although attempts were made to remove these impurities through degassing for this study, it is important to note that struvite precipitation and dissolution will occur in organic-rich wastewater. Organic matter typically acts as an inhibitor both in terms of extent of P removal and precipitation kinetics in struvite crystallization systems. The strength of the effect is dependent on the type of organic matter (particulate, colloidal, or dissolved) and increases as reactor pH drops below 9.[60,66,67] Other evidence shows that organic matter can cause morphology changes that could result in differences in an overall dissolution rate.[67] In contrast, one study suggests that certain phenolic groups may actually accelerate nucleation and growth rates and counteract calcium-related morphology changes.[68] This conflicting empirical evidence is partially reconciled by a mechanistic study that shows struvite−organic interactions are adsorption-driven and thus will differ between adsorbents with various interfacial energies.[69] Current quantitative methods to capture the influence of organic matter on struvite are limited to overall P removal crystallization process models based on the modified Monod equation.[67] The benefit of using the SOM for dissolution kinetics is that by including an empirical saturation constant (C_{sat}), a specific plant can easily calibrate dissolution kinetics (k—SOM dissolution rate constant) by performing solubility jar tests and couple that to expected or measured product crystal sizes to calculate expected dissolution rates.

Not addressed in this work are other potential P sinks that form by dosing iron or aluminum salts for chemical P control,[70] as a coagulant,[71] or as a side effect of dosing iron for sulfide control[72] in anaerobic reducing environments like those found during solids treatment or in collection systems. The most prevalent iron phase observed to form at iron-dosed WRRFs is vivianite ($Fe_2(PO_4)_2{\cdot}8H_2O$), which has a very low solubility (pK_{sp} = 36)[73] comparable to a mineral like hydroxyapatite. Some samples have shown that more than 90% of all P in digested sludge can be attributed to vivianite when iron is dosed in the mainstream treatment process for phosphorus removal.[74] In this study, EBPR was the primary P removal strategy in the mainstream. As a result, substantial

https://doi.org/10.1021/acsestengg.1c00404
ACS EST Engg. 2022, 2, 874−885

soluble P rather than vivianite is shown exiting the anaerobic digester (Figures S5 and S6) and routed either to the crystallizer or removed from the plant in the biosolids. Future research could account for the plantwide dynamics of vivianite when iron dosing is used for P removal using the experimental and modeling framework presented here.

Similarly, while included in the activated sludge model used in this study, little focus was put on the formation of calcium phosphates—a common co-precipitant alongside vivianite (when iron is present) in struvite crystallization systems.[74,75] The effects of calcium on struvite are best seen in animal wastes,[76−78] where baseline calcium concentrations are much higher than in wastewater and result in the scavenging of P forming kinetically favored ACP and can eventually lead to the formation of thermodynamically stable hydroxyapatite.[79−81] Roughly, 4% of the P solids seen in Figure 5C,D are ACP formed during EBPR from influent calcium. Also of concern is heavy metal adsorption on struvite as the known inhibition of growth kinetics is likely to continue during dissolution.[82] The interactions between struvite solids and inorganic species are ubiquitous and point toward a need for a further understanding of the role each phase plays in the plantwide treatment processes.

4. OUTLOOK

Due to the increased implementation of struvite crystallization systems across North America and in Europe and the observed washout of fines, a better understanding of the kinetics of dissolution for struvite is necessary for accurate modeling and simulation of plantwide processes related to P removal and recovery. This work addresses this need by (1) fitting new struvite dissolution kinetic data as a function of struvite particle size to the SOM and (2) providing insights into the plantwide implications of struvite loss from sidestream precipitation reactors through process modeling and simulation in SUMO. These results show a clear change in plant performance both in terms of effluent P and the phase/stream, where P is discharged when particle size is considered.

The next important step in verifying the results shown here is calibration and validation with real plantwide data. More data on particle size distributions is needed from crystallizer effluents during washout and from primary clarifiers to determine which particles survive dissolution. Second, future attempts at understanding plantwide fines dynamics should be made including crystallizer-specific process models[23−25,28,42] and hydrodynamics to better simulate when fines will be generated and when washout can be expected. However, the less understood effect of organics and coprecipitates (ACP and brushite) on the struvite crystallization process is another missing component in these well-developed process models that exists in practice. A combination of isolated process experiments and calibration to real-world reactors could address this issue.

Future struvite crystallizer design will be informed by an additional feedback loop related to fines removal costs that could lead to a new target particle size or even introduction of new mechanism-specific zones (i.e. nucleation, crystal growth, and agglomeration) and crystallizer conditions (low saturation, high mixing, etc.). As the introduction of crystallizer technologies becomes more prevalent, accounting for dissolution of fines could become a necessary part of accurate modeling and simulation, especially for systems where upsets occur that result in a significant transfer of P to mainstream treatment processes as struvite fines.

■ ASSOCIATED CONTENT

Supporting Information

The Supporting Information is available free of charge at https://pubs.acs.org/doi/10.1021/acsestengg.1c00404.

XRD and FTIR characterization of field-grown samples, calculated saturation index of various P-containing solids under batch dissolution conditions, simulated effluent quality during P breakthrough due to low influent BOD/P, Sankey diagrams showing P flow and transformations throughout the simulated plant for 1000 and 200 μm struvite fines lost from the crystallizer, Sumo1 influent state variable values used in this study, operating/design parameters used in the plantwide simulations, and summary of effluent quality for 1000 and 200 μm fines at yields typical of regular crystallizer operation (PDF)

■ AUTHOR INFORMATION

Corresponding Author

Roland D. Cusick − *Department of Civil and Environmental Engineering, 3217 Newmark Civil Engineering Laboratory, University of Illinois at Urbana-Champaign, Urbana, Illinois 61801, United States;* orcid.org/0000-0002-4037-2939; Phone: +1 217-224-6727; Email: rcusick@illinois.edu

Authors

Samuel E. Aguiar − *Department of Civil and Environmental Engineering, 3217 Newmark Civil Engineering Laboratory, University of Illinois at Urbana-Champaign, Urbana, Illinois 61801, United States;* orcid.org/0000-0002-2803-2106

Manying Zhang − *Department of Civil and Environmental Engineering, 3217 Newmark Civil Engineering Laboratory, University of Illinois at Urbana-Champaign, Urbana, Illinois 61801, United States*

Adrian Romero-Flores − *Jacobs Engineering, Charlotte, North Carolina 28277, United States*

Tom Johnson − *Jacobs Engineering, Charlotte, North Carolina 28277, United States*

Complete contact information is available at: https://pubs.acs.org/10.1021/acsestengg.1c00404

Notes

The authors declare no competing financial interest.

■ ACKNOWLEDGMENTS

All XRD studies were carried out in part at the Materials Research Laboratory Central Research Facilities, University of Illinois. This work was funded by the US National Science Foundation award no. 1739788 entitled "INFEWS/T1: Advancing FEW System Resilience in the Corn Belt by Integrated Technology-Environment-Economics Modeling of Nutrient Cycling." The authors would also like to acknowledge personnel from Ostara Nutrient Recovery Technologies Inc., CWS, Stickney, and MWRD for providing the field-grown struvite samples used in this study. Finally, we acknowledge Rachel Lee and Mikaela Verigin from Ostara Nutrient Recovery Technologies Inc. and Leon Downing from Black and Veatch for their discussion on the general scope and applicability of this study in industries.

REFERENCES

(1) US EPA. State Progress Toward Developing Numeric Nutrient Water Quality Criteria for Nitrogen and Phosphorus. https://www.epa.gov/nutrient-policy-data/state-progress-toward-developing-numeric-nutrient-water-quality-criteria (accessed May 09, 2021).

(2) Desmidt, E.; Ghyselbrecht, K.; Zhang, Y.; Pinoy, L.; Van der Bruggen, B.; Verstraete, W.; Rabaey, K.; Meesschaert, B. Global Phosphorus Scarcity and Full-Scale P-Recovery Techniques: A Review. *Crit. Rev. Environ. Sci. Technol.* **2015**, *45*, 336−384.

(3) Santos, A. F.; Almeida, P. V.; Alvarenga, P.; Gando-Ferreira, L. M.; Quina, M. J. From Wastewater to Fertilizer Products: Alternative Paths to Mitigate Phosphorus Demand in European Countries. *Chemosphere* **2021**, *284*, 131258.

(4) Jupp, A. R.; Beijer, S.; Narain, G. C.; Schipper, W.; Slootweg, J. C. Phosphorus recovery and recycling - closing the loop. *Chem. Soc. Rev.* **2021**, *50*, 87−101.

(5) Mihelcic, J. R.; Fry, L. M.; Shaw, R. Global Potential of Phosphorus Recovery from Human Urine and Feces. *Chemosphere* **2011**, *84*, 832−839.

(6) Münch, E. V.; Barr, K. Controlled Struvite Crystallisation for Removing Phosphorus from Anaerobic Digester Sidestreams. *Water Res.* **2001**, *35*, 151−159.

(7) Kassouf, H.; García Parra, A.; Mulford, L.; Iranipour, G.; Ergas, S. J.; Cunningham, J. A. Mass Fluxes of Nitrogen and Phosphorus through Water Reclamation Facilities: Case Study of Biological Nutrient Removal, Aerobic Sludge Digestion, and Sidestream Recycle. *Water Environ. Res.* **2020**, *92*, 478−489.

(8) Hukari, S.; Hermann, L.; Nättorp, A. From wastewater to fertilisers—Technical overview and critical review of European legislation governing phosphorus recycling. *Sci. Total Environ.* **2016**, *542*, 1127−1135.

(9) Tomei, M. C.; Stazi, V.; Daneshgar, S.; Capodaglio, A. G. Holistic Approach to Phosphorus Recovery from Urban Wastewater: Enhanced Biological Removal Combined with Precipitation. *Sustainability* **2020**, *12*, 575.

(10) Sena, M.; Hicks, A. Life Cycle Assessment Review of Struvite Precipitation in Wastewater Treatment. *Resour., Conserv. Recycl.* **2018**, *139*, 194−204.

(11) Shu, L.; Schneider, P.; Jegatheesan, V.; Johnson, J. An Economic Evaluation of Phosphorus Recovery as Struvite from Digester Supernatant. *Bioresour. Technol.* **2006**, *97*, 2211−2216.

(12) Blackall, L. L.; Crocetti, G. R.; Saunders, A. M.; Bond, P. L. A Review and Update of the Microbiology of Enhanced Biological Phosphorus Removal in Wastewater Treatment Plants. *Antonie van Leeuwenhoek* **2002**, *81*, 681−691.

(13) Agrawal, S.; Guest, J. S.; Cusick, R. D. Elucidating the Impacts of Initial Supersaturation and Seed Crystal Loading on Struvite Precipitation Kinetics, Fines Production, and Crystal Growth. *Water Res.* **2018**, *132*, 252−259.

(14) Le Corre, K. S.; Valsami-Jones, E.; Hobbs, P.; Parsons, S. A. Impact of Calcium on Struvite Crystal Size, Shape and Purity. *J. Cryst. Growth* **2005**, *283*, 514−522.

(15) Tarragó, E.; Puig, S.; Ruscalleda, M.; Balaguer, M. D.; Colprim, J. Controlling struvite particles' size using the up-flow velocity. *Chem. Eng. J.* **2016**, *302*, 819−827.

(16) Ronteltap, M.; Maurer, M.; Hausherr, R.; Gujer, W. Struvite precipitation from urine—Influencing factors on particle size. *Water Res.* **2010**, *44*, 2038−2046.

(17) Hanhoun, M.; Montastruc, L.; Azzaro-Pantel, C.; Biscans, B.; Frèche, M.; Pibouleau, L. Simultaneous Determination of Nucleation and Crystal Growth Kinetics of Struvite Using a Thermodynamic Modeling Approach. *Chem. Eng. J.* **2013**, *215−216*, 903−912.

(18) Polat, S.; Sayan, P. Application of response surface methodology with a Box-Behnken design for struvite precipitation. *Adv. Powder Technol.* **2019**, *30*, 2396−2407.

(19) Le Corre, K. S.; Valsami-Jones, E.; Hobbs, P.; Jefferson, B.; Parsons, S. A. Agglomeration of Struvite Crystals. *Water Res.* **2007**, *41*, 419−425.

(20) Li, B.; Boiarkina, I.; Young, B.; Yu, W. Quantification and Mitigation of the Negative Impact of Calcium on Struvite Purity. *Adv. Powder Technol.* **2016**, *27*, 2354−2362.

(21) Mehta, C. M.; Batstone, D. J. Nucleation and Growth Kinetics of Struvite Crystallization. *Water Res.* **2013**, *47*, 2890−2900.

(22) Triger, A.; Pic, J.-S.; Cabassud, C. Determination of Struvite Crystallization Mechanisms in Urine Using Turbidity Measurement. *Water Res.* **2012**, *46*, 6084−6094.

(23) Elduayen-Echave, B.; Lizarralde, I.; Larraona, G. S.; Ayesa, E.; Grau, P. A New Mass-Based Discretized Population Balance Model for Precipitation Processes: Application to Struvite Precipitation. *Water Res.* **2019**, *155*, 26−41.

(24) Galbraith, S. C.; Schneider, P. A.; Flood, A. E. Model-Driven Experimental Evaluation of Struvite Nucleation, Growth and Aggregation Kinetics. *Water Res.* **2014**, *56*, 122−132.

(25) Burns, M.; Sheehan, M.; Schneider, P. A. Nucleation and Crystal Growth Kinetic Parameter Optimization of a Continuous Poiseuille Flow Struvite Crystallizer Using a Discretized Population Balance and Dynamic Fluid Model. *Chem. Eng. J.* **2021**, *405*, 126607.

(26) Battistoni, P.; Fava, G.; Pavan, P.; Musacco, A.; Cecchi, F. Phosphate Removal in Anaerobic Liquors by Struvite Crystallization without Addition of Chemicals: Preliminary Results. *Water Res.* **1997**, *31*, 2925−2929.

(27) Battistoni, P.; Pavan, P.; Prisciandaro, M.; Cecchi, F. Struvite Crystallization: A Feasible and Reliable Way to Fix Phosphorus in Anaerobic Supernatants. *Water Res.* **2000**, *34*, 3033−3041.

(28) Elduayen-Echave, B.; Lizarralde, I.; Schneider, P. A.; Ayesa, E.; Larraona, G. S.; Grau, P. Inclusion of Shear Rate Effects in the Kinetics of a Discretized Population Balance Model: Application to Struvite Precipitation. *Water Res.* **2021**, *200*, 117242.

(29) Ye, X.; Ye, Z.-L.; Lou, Y.; Pan, S.; Wang, X.; Wang, M. K.; Chen, S. A Comprehensive Understanding of Saturation Index and Upflow Velocity in a Pilot-Scale Fluidized Bed Reactor for Struvite Recovery from Swine Wastewater. *Powder Technol.* **2016**, *295*, 16−26.

(30) Xu, K.; Ge, L.; Wang, C. Effect of Upflow Velocity on the Performance of a Fluidized Bed Reactor to Remove Phosphate from Simulated Swine Wastewater. *Int. Biodeterior. Biodegrad.* **2019**, *140*, 78−83.

(31) Zamora, P.; Georgieva, T.; Salcedo, I.; Elzinga, N.; Kuntke, P.; Buisman, C. J. Long-Term Operation of a Pilot-Scale Reactor for Phosphorus Recovery as Struvite from Source-Separated Urine. *J. Chem. Technol. Biotechnol.* **2017**, *92*, 1035−1045.

(32) Crutchik, D.; Morales, N.; Vázquez-Padín, J. R.; Garrido, J. M. Enhancement of Struvite Pellets Crystallization in a Full-Scale Plant Using an Industrial Grade Magnesium Product. *Water Sci. Technol.* **2016**, *75*, 609−618.

(33) Saerens, B.; Geerts, S.; Weemaes, M. Phosphorus recovery as struvite from digested sludge - experience from the full scale. *J. Environ. Manage.* **2021**, *280*, 111743.

(34) Romero, A.; Johnson, T. D.; Downing, L.; Menniti, A.; Leaf, W.; Seib, M.; Gearhart, R.; Fitzgerald, C. Lost Crystals- Impacts of Struvite Recovery Performance on Plant Capacity for Achieving Low-P Effluent. *Proceedings of the Water Environment Federation*; Water Environment Federation, 2018; Vol. *2018*, pp 511−516. DOI: 10.2175/193864718824940105

(35) Kazadi Mbamba, C.; Batstone, D. J.; Flores-Alsina, X.; Tait, S. A Generalised Chemical Precipitation Modelling Approach in Wastewater Treatment Applied to Calcite. *Water Res.* **2015**, *68*, 342−353.

(36) Koutsoukos, P.; Amjad, Z.; Tomson, M. B.; Nancollas, G. H. Crystallization of Calcium Phosphates. A Constant Composition Study. *J. Am. Chem. Soc.* **1980**, *102*, 1553−1557.

(37) Musvoto, E.; Wentzel, M. C.; Loewenthal, R. E.; Ekama, G. A. Integrated chemicalâ€″physical processes modellingâ€″I. Development of a kinetic-based model for mixed weak acid/base systems. *Water Res.* **2000**, *34*, 1857−1867.

(38) Aagaard, P.; Helgeson, H. C. Thermodynamic and Kinetic Constraints on Reaction Rates among Minerals and Aqueous

https://doi.org/10.1021/acsestengg.1c00404
ACS EST Engg. 2022, 2, 874−885

Solutions; I, Theoretical Considerations. *Am. J. Sci.* **1982**, *282*, 237−285.
(39) Bouropoulos, N. C.; Koutsoukos, P. G. Spontaneous Precipitation of Struvite from Aqueous Solutions. *J. Cryst. Growth* **2000**, *213*, 381−388.
(40) Ohlinger, K. N.; E, P.; Young, T. M.; Schroeder, E. D. Kinetics Effects on Preferential Struvite Accumulation in Wastewater. *J. Environ. Eng.* **1999**, *125*, 730−737.
(41) Hounslow, M. J.; Ryall, R. L.; Marshall, V. R. A Discretized Population Balance for Nucleation, Growth, and Aggregation. *AIChE J.* **1988**, *34*, 1821−1832.
(42) Galbraith, S. C.; Schneider, P. A. Modelling and Simulation of Inorganic Precipitation with Nucleation, Crystal Growth and Aggregation: A New Approach to an Old Method. *Chem. Eng. J.* **2014**, *240*, 124−132.
(43) Henze, M.; Gujer, W.; Mino, T.; van Loosdrecht, M. C. *Activated Sludge Models ASM1, ASM2, ASM2d and ASM3*; IWA Publishing: London, 2000.
(44) Truesdale, V. W.; Greenwood, J. Latent Disciplinal Clashes Concerning the Batch Dissolution of Minerals, and Their Wider Implications. *Environ. Chem.* **2018**, *15*, 113.
(45) Dynamita. *SUMO. Dynamita: Nyons*, France, 2019.
(46) Bhuiyan, M. I. H.; Mavinic, D. S.; Koch, F. A. Thermal Decomposition of Struvite and Its Phase Transition. *Chemosphere* **2008**, *70*, 1347−1356.
(47) Gustafsson, J. P. *Visual MINTEQ*, Ver 3.1; KTH: Sweden, 2020. https://vminteq.lwr.kth.se/(accessed May 09, 2021).
(48) Taylor, A. W.; Frazier, A. W.; Gurney, E. L.; Smith, J. P. Solubility Products of Di- and Trimagnesium Phosphates and the Dissociation of Magnesium Phosphate Solutions. *Trans. Faraday Soc.* **1963**, *59*, 1585.
(49) Burton, F. L.; Tchobanoglous, G.; Tsuchihashi, R.; Stensel, H. D.; Metcalf & Eddy Inc. *Wastewater Engineering: Treatment and Resource Recovery*, 5th ed.; McGraw-Hill Education: New York, NY, 2013.
(50) Dietrich, W. E. Settling Velocity of Natural Particles. *Water Resour. Res.* **1982**, *18*, 1615−1626.
(51) Schaum, C.; Gysin, A.; Lycke, D.; Wirtel, S. The Pearl and WASSTRIP Processes (Canada). *Phosphorus: Polluter and Resource of the Future: Motivations, Technologies and Assessment of the Elimination and Recovery of Phosphorus from Wastewater*; IWA Publishing: London, 2018; p 590.
(52) Le Corre, K. S.; Valsami-Jones, E.; Hobbs, P.; Parsons, S. A. Phosphorus Recovery from Wastewater by Struvite Crystallization: A Review. *Crit. Rev. Environ. Sci. Technol.* **2009**, *39*, 433−477.
(53) Rahman, M. M.; Salleh, M. A. M.; Rashid, U.; Ahsan, A.; Hossain, M. M.; Ra, C. S. Production of slow release crystal fertilizer from wastewaters through struvite crystallization—A review. *Arab. J. Chem.* **2014**, *7*, 139−155.
(54) Xu, K.; Li, J.; Zheng, M.; Zhang, C.; Xie, T.; Wang, C. The Precipitation of Magnesium Potassium Phosphate Hexahydrate for P and K Recovery from Synthetic Urine. *Water Res.* **2015**, *80*, 71−79.
(55) Graeser, S.; Postl, W.; Bojar, H.-P. B.; Armbruster, T.; Raber, T.; Ettinger, K.; Walter, F. Struvite-(K), KMgPO46H2O, the potassium equivalent of struvite a new mineral. *Eur. J. Mineral.* **2008**, *20*, 629−633.
(56) Wilsenach, J. A.; Schuurbiers, C. A. H.; van Loosdrecht, M. C. M. Phosphate and Potassium Recovery from Source Separated Urine through Struvite Precipitation. *Water Res.* **2007**, *41*, 458−466.
(57) Lee, S.-H.; Yoo, B.-H.; Lim, S. J.; Kim, T.-H.; Kim, S.-K.; Kim, J. Y. Development and Validation of an Equilibrium Model for Struvite Formation with Calcium Co-Precipitation. *J. Cryst. Growth* **2013**, *372*, 129−137.
(58) Liu, X.; Wang, J. Impact of Calcium on Struvite Crystallization in the Wastewater and Its Competition with Magnesium. *Chem. Eng. J.* **2019**, *378*, 122121.
(59) Li, B.; Huang, H. M.; Boiarkina, I.; Yu, W.; Huang, Y. F.; Wang, G. Q.; Young, B. R. Phosphorus Recovery through Struvite Crystallisation: Recent Developments in the Understanding of Operational Factors. *J. Environ. Manage.* **2019**, *248*, 109254.
(60) Muhmood, A.; Wang, X.; Dong, R.; Wu, S. New Insights into Interactions of Organic Substances in Poultry Slurry with Struvite Formation: An Overestimated Concern? *Sci. Total Environ.* **2021**, *751*, 141789.
(61) Liu, J. D.; Xu, Z. X.; Wang, W. G.; Jin, W. The Effect of Organic Compounds on the Recovery of Ammonium by Struvite Precipitation from Swine Anaerobic Digester Effluent. *Adv. Mater. Res.* **2013**, *610−613*, 2350−2355.
(62) Ungár, T. Microstructural Parameters from X-Ray Diffraction Peak Broadening. *Scr. Mater.* **2004**, *51*, 777−781.
(63) Han, Z.; Zhao, Y.; Yan, H.; Zhao, H.; Han, M.; Sun, B.; Sun, X.; Hou, F.; Sun, H.; Han, L.; Sun, Y.; Wang, J.; Li, H.; Wang, Y.; Du, H. Struvite Precipitation Induced by a Novel Sulfate-Reducing BacteriumAcinetobacter calcoaceticusSRB4 Isolated from River Sediment. *Geomicrobiol. J.* **2015**, *32*, 868−877.
(64) Larkin, P. IR and Raman Spectra-Structure Correlations. In *Infrared and Raman Spectroscopy*; Larkin, P., Ed.; Elsevier: Oxford, 2011; pp 73−115.
(65) Abbona, F.; Boistelle, R. Growth morphology and crystal habit of struvite crystals (MgNH4PO4 · 6 H2O). *J. Cryst. Growth* **1979**, *46*, 339−354.
(66) Capdevielle, A.; Sýkorová, E.; Béline, F.; Daumer, M.-L. Effects of Organic Matter on Crystallization of Struvite in Biologically Treated Swine Wastewater. *Environ. Technol.* **2016**, *37*, 880−892.
(67) Zhou, Z.; Hu, D.; Ren, W.; Zhao, Y.; Jiang, L.-M.; Wang, L. Effect of Humic Substances on Phosphorus Removal by Struvite Precipitation. *Chemosphere* **2015**, *141*, 94−99.
(68) Rabinovich, A.; Rouff, A. A. Effect of Phenolic Organics on the Precipitation of Struvite from Simulated Dairy Wastewater. *ACS ES&T Water* **2021**, *1*, 910−918.
(69) Li, H.; Zhao, T.-L.; Qian, F.-J.; Jiang, H.-F.; Yao, Q.-Z.; Luo, Y.; Fu, S.-Q.; Zhou, G.-T. A Model of Extracellular Polymeric Substances on Crystal Growth and Morphogenesis of Struvite: Effects of Sodium Alginate. *Powder Technol.* **2021**, *380*, 80−88.
(70) Szabó, A.; Takács, I.; Murthy, S.; Daigger, G. T.; Licskó, I.; Smith, S. Significance of Design and Operational Variables in Chemical Phosphorus Removal. *Water Environ. Res.* **2008**, *80*, 407−416.
(71) Li, J. Effects of Fe(III) on Floc Characteristics of Activated Sludge. *J. Chem. Technol. Biotechnol.* **2005**, *80*, 313−319.
(72) Gutierrez, O.; Park, D.; Sharma, K. R.; Yuan, Z. Iron Salts Dosage for Sulfide Control in Sewers Induces Chemical Phosphorus Removal during Wastewater Treatment. *Water Res.* **2010**, *44*, 3467−3475.
(73) Wilfert, P.; Kumar, P. S.; Korving, L.; Witkamp, G.-J.; van Loosdrecht, M. C. M. The Relevance of Phosphorus and Iron Chemistry to the Recovery of Phosphorus from Wastewater: A Review. *Environ. Sci. Technol.* **2015**, *49*, 9400−9414.
(74) Wilfert, P.; Dugulan, A. I.; Goubitz, K.; Korving, L.; Witkamp, G. J.; Van Loosdrecht, M. C. M. Vivianite as the Main Phosphate Mineral in Digested Sewage Sludge and Its Role for Phosphate Recovery. *Water Res.* **2018**, *144*, 312−321.
(75) Margenot, A. J.; Kitt, D.; Gramig, B. M.; Berkshire, T. B.; Chatterjee, N.; Hertzberger, A. J.; Aguiar, S.; Furneaux, A.; Sharma, N.; Cusick, R. D. Toward a Regional Phosphorus (Re)Cycle in the US Midwest. *J. Environ. Qual.* **2019**, *48*, 1397−1413.
(76) Shen, Y.; Ogejo, J. A.; Bowers, K. E. Abating the Effects of Calcium on Struvite Precipitation in Liquid Dairy Manure. *Trans. ASABE* **2011**, *54*, 325−336.
(77) Zhang, T.; Bowers, K. E.; Harrison, J. H.; Chen, S. Releasing Phosphorus from Calcium for Struvite Fertilizer Production from Anaerobically Digested Dairy Effluent. *Water Environ. Res.* **2010**, *82*, 34−42.
(78) Huchzermeier, M. P.; Tao, W. Overcoming Challenges to Struvite Recovery from Anaerobically Digested Dairy Manure. *Water Environ. Res.* **2012**, *84*, 34−41.

https://doi.org/10.1021/acsestengg.1c00404
ACS EST Engg. 2022, 2, 874−885

(79) Dey, A.; Bomans, P. H. H.; Müller, F. A.; Will, J.; Frederik, P. M.; de With, G.; Sommerdijk, N. A. The Role of Prenucleation Clusters in Surface-Induced Calcium Phosphate Crystallization. *Nat. Mater.* **2010**, *9*, 1010.
(80) Uskoković, V. Disordering the Disorder as the Route to a Higher Order: Incoherent Crystallization of Calcium Phosphate through Amorphous Precursors. *Cryst. Growth Des.* **2019**, *19*, 4340−4357.
(81) Habraken, W. J. E. M.; Tao, J.; Brylka, L. J.; Friedrich, H.; Bertinetti, L.; Schenk, A. S.; Verch, A.; Dmitrovic, V.; Bomans, P. H. H.; Frederik, P. M.; Laven, J.; van der Schoot, P.; Aichmayer, B.; de With, G.; DeYoreo, J. J.; Sommerdijk, N. A. J. M. Ion-Association Complexes Unite Classical and Non-Classical Theories for the Biomimetic Nucleation of Calcium Phosphate. *Nat. Commun.* **2013**, *4*, 1507.
(82) Liu, X.; Wang, Y.; Chang, J. A Review on the Incorporation and Potential Mechanism of Heavy Metals on the Recovered Struvite from Wastewater. *Water Res.* **2021**, *207*, 117823.

https://doi.org/10.1021/acsestengg.1c00404
ACS EST Engg. 2022, 2, 874−885